DAO1 catalyzes temporal and tissue-specific oxidative inactivation of auxin in *Arabidopsis thaliana*

Jun Zhang[a], Jinshan Ella Lin[b,c], Chinchu Harris[a], Fernanda Campos Mastrotti Pereira[d,e], Fan Wu[d], Joshua J. Blakeslee[b,c], and Wendy Ann Peer[a,d,1]

[a]Department of Plant Science and Landscape Architecture, University of Maryland, College Park, MD 20742; [b]Department of Horticulture and Crop Science, Ohio Agricultural Research and Development Center, The Ohio State University, Wooster, OH 44691; [c]Ohio Agricultural Research and Development Center Metabolite Analysis Cluster, Ohio Agricultural Research and Development Center, The Ohio State University, Wooster, OH 44691; [d]Department of Environmental Science and Technology, University of Maryland, College Park, MD 20742; and [e]Plant Protection and Animal Health, Forestry, Agronomy, Universidade Estadual de São Paulo, Sao Paulo, Brazil

Edited by Mark Estelle, University of California at San Diego, La Jolla, CA, and approved July 29, 2016 (received for review March 22, 2016)

Tight homeostatic regulation of the phytohormone auxin [indole-3-acetic acid (IAA)] is essential to plant growth. Auxin biosynthetic pathways and the processes that inactivate auxin by conjugation to amino acids and sugars have been thoroughly characterized. However, the enzyme that catalyzes oxidation of IAA to its primary catabolite 2-oxindole-3-acetic acid (oxIAA) remains uncharacterized. Here, we show that DIOXYGENASE FOR AUXIN OXIDATION 1 (DAO1) catalyzes formation of oxIAA in vitro and in vivo and that this mechanism regulates auxin homeostasis and plant growth. Null *dao1-1* mutants contain 95% less oxIAA compared with wild type, and complementation of *dao1* restores wild-type oxIAA levels, indicating that DAO1 is the primary IAA oxidase in seedlings. Furthermore, *dao1* loss of function plants have altered morphology, including larger cotyledons, increased lateral root density, delayed sepal opening, elongated pistils, and reduced fertility in the primary inflorescence stem. These phenotypes are tightly correlated with *DAO1* spatiotemporal expression patterns as shown by *DAO1pro*:β-glucuronidase (GUS) activity and *DAO1pro*:YFP-DAO1 signals, and transformation with *DAO1pro*:YFP-DAO1 complemented the mutant phenotypes. The dominant *dao1-2D* mutant has increased oxIAA levels and decreased stature with shorter leaves and inflorescence stems, thus supporting DAO1 IAA oxidase function in vivo. A second isoform, DAO2, is very weakly expressed in seedling root apices. Together, these data confirm that IAA oxidation by DAO1 is the principal auxin catabolic process in *Arabidopsis* and that localized IAA oxidation plays a role in plant morphogenesis.

auxin homeostasis | auxin oxidation | auxin oxidase | lateral roots | flowers

The phytohormone auxin [indole-3-acetic acid (IAA)] regulates plant architecture, tropic growth, and multiple other aspects of plant development. The spatiotemporal distribution of auxin is regulated at the cellular level by control of biosynthesis, transport, reversible conjugation, compartmentalization, and catabolism. Loss of any one of these mechanisms is often balanced by compensatory homeostatic responses but can also produce morphological or physiological changes. The enzymes that catalyze auxin biosynthesis via the indole-3-pyruvic acid (IPyA) pathway (1, 2) and the UDP-glucose transferases (3–5) and amido synthetases that inactivate IAA by conjugation to small molecules (6, 7) are well-characterized (Fig. 1*A*). Most IAA conjugation is reversible and functions in compartmentation or storage (7–9). Exceptions are the formation of the irreversible catabolites indole-3-acetic acid-aspartic acid (IAA-Asp) and indole-3-acetic acid-glutamic acid (IAA-Glu) in discrete plant tissues (10–12).

Oxidation of IAA has long been known to be the primary mechanism of auxin catabolism (13). *Arabidopsis* seedlings contain 10–100 times more 2-oxindole-3-acetic acid (oxIAA) than the major IAA conjugates IAA-Glu and IAA-Asp (10, 14, 15), but the enzymes catalyzing oxIAA formation have been elusive. In part, this has been because of early implication of peroxidases and oxygenases in auxin oxidative processes (13, 16–18). However, reexamination by liquid chromatography-mass spectrometry (LC-MS) of the reaction products from previously published horseradish and grape leaf peroxidases as well as two *Arabidopsis* peroxidases showed that these reactions produce the decarboxylation products indole-3-carbinol, 3-methylene-2-oxindole, and 3-hydroxymethyl-2-oxindole present in low levels in plants (19) but not oxIAA (20). In *Zea mays*, oxIAA was reported to be produced by an oxygen-requiring soluble enzyme and a more active detergent-soluble, stable component (17). A correlation of cellular oxIAA and IAA levels (15, 20) and with expression of a gene with similarity to a rice gene named *DIOXYGENASE FOR AUXIN OXIDATION* (*DAO*) (21, 22) and sequence homology to apple *ADVENTITIOUS ROOTING RELATED OXYGENASE 1* (23) suggested that similar genes in *Arabidopsis*, *DAO1* and *DAO2*, encode the enzymes that produce oxIAA (24, 25). Here, we show that DAO1 and DAO2 catalyze oxIAA formation and that DAO1 is the major IAA oxidase in *Arabidopsis*. The temporal- and tissue-specific oxidative inactivation of auxin by DAO fine tunes IAA levels throughout the life of the plant to maintain optimal growth and development.

Phylogenetic Analysis of *Arabidopsis* 2-Oxoglutarate and Fe(II)-Dependent Oxygenase Superfamily

Previous work from our laboratory suggested that oxIAA formation was catalyzed by a member of the 2-oxoglutarate and Fe(II)-dependent [2OG Fe(II)] oxygenase superfamily (20).

Significance

Although auxin oxidation has long been known to be the primary mechanism of auxin catabolism and *Arabidopsis* seedlings have 10–100 more 2-oxindole 3-acetic acid compared with other auxin catabolic products, the enzymes that constitutively catalyze this process remained unknown. This work fills the gap by identifying and characterizing the *Arabidopsis* proteins DIOXYGENASE FOR AUXIN OXIDATION 1 (DAO1) and DAO2, which catalyze auxin oxidation under normal growth conditions and shows that this activity has a physiological function in planta. The protein localization and phenotypes of the loss/gain of function mutants support that DAO1 is the primary constitutive mechanism of auxin catabolism in *Arabidopsis* and that the temporal- and tissue-specific oxidative inactivation of auxin by DAO adjusts indole-3-acetic acid levels throughout the life of the plant to optimize growth and development.

Author contributions: J.Z. and W.A.P. designed research; J.Z., J.E.L., C.H., F.C.M.P., F.W., J.J.B., and W.A.P. performed research; J.Z., J.E.L., F.C.M.P., J.J.B., and W.A.P. analyzed data; and J.Z., J.E.L., J.J.B., and W.A.P. wrote the paper.

The authors declare no conflict of interest.

This article is a PNAS Direct Submission.

Freely available online through the PNAS open access option.

See Commentary on page 10742.

[1]To whom correspondence should be addressed. Email: wapeer@umd.edu.

This article contains supporting information online at www.pnas.org/lookup/suppl/doi:10.1073/pnas.1604769113/-/DCSupplemental.

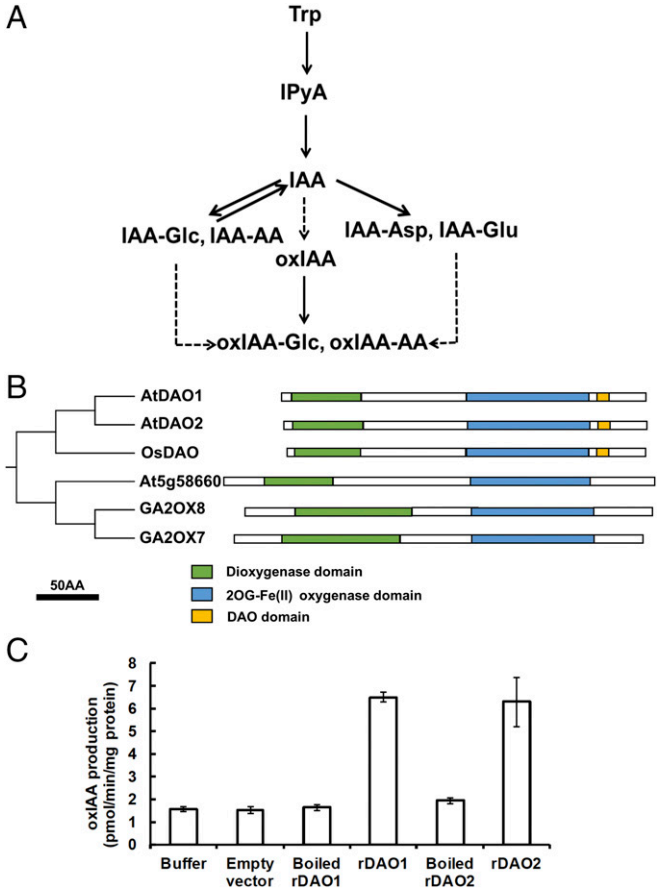

Fig. 1. Identification and characterization of 2-oxindole acetic acid synthetases in *A. thaliana*. (*A*) Simplified auxin metabolic pathway via IPyA. IAA-AA, indole-3-acetic acid-amino acid conjugate; IAA-Glc, indole-3-acetic acid-glucose; oxIAA-AA, 2-oxindole-3-acetic acid-amino acid conjugate; oxIAA-Glc, 2-oxindole-3-acetic acid-glucose; Trp, tryptophan. (*B*) Pictogram of conserved domains among OsDAO, AtDAO1, AtDAO2, and the nearest clade of a subfamily of 2-oxoglutarate oxygenases in *Arabidopsis*. (*C*) Enzyme assays of rDAO (rDAO1 and rDAO2) with buffer control, empty vector control, and heat-inactivated (boiled) enzyme control with IAA as a substrate. Data are means ± SD of at least independent 10 experiments.

AtDAO1 (At1g14130) and AtDAO2 (At1g14120) in *Arabidopsis thaliana* were identified as homologs of rice OsDAO (Os04g0475600) (Fig. S1); all members of this superfamily are characterized by the conserved dioxygenase and 2OG Fe(II) oxygenase domains (Fig. 1*B* and Fig. S1). Another conserved sequence P(S/D/G)E (F/L)VD(A/G)EHPR without any known motifs was identified among the rice and *Arabidopsis* DAO proteins and examined further (Fig. 1*B* and Fig. S1). Sequence alignment with Viridiplantae (taxid: 33090) suggests that this motif is specific to proteins in a subset of the 2OG Fe(II) oxygenase superfamily annotated as DAO and DAO like (Table S1). Motif analysis (26, 27) also showed μ-Adaptor Protein and actin binding motifs (Fig. S1), 12 putative serine/threonine phosphorylation sites in DAO1, and 15 sites in DAO2.

The majority of the proteins in the 2OG Fe(II) oxygenase superfamily have not been characterized, and a phylogenetic analysis of the superfamily in *Arabidopsis* was undertaken to identify any nearest neighbors to DAO1 and DAO2 (Fig. S2) (24). The nearest neighbors are AT5G58660, an uncharacterized gene, AT1G50960 (GA2OX7), and AT4G21200 (GA2OX8), all of which lack the DAO motif (Fig. 1*B*). Similarly, Porco et al. (24) report that DAO1/2 are in a separate clade closest to GAOX7/8.

Recombinant DAO Can Catalyze the Formation of oxIAA

To test the hypothesis that DAO1 and/or DAO2 catalyze the oxidation of IAA into oxIAA, enzyme assays were conducted with recombinant DIOXYGENASE FOR AUXIN OXIDATION (rDAO; 36 kDa) (Fig. S3 and Table S2) and IAA as a substrate. Ultra performance liquid chromatography (UPLC) and LC-MS/MS were used to analyze the products from in vitro enzyme assays, wherein IAA was incubated with purified rDAO1 or rDAO2. In both cases, one major peak with the same retention time and mass transitions as the oxIAA standard was observed (Fig. S4), with low background levels of oxIAA (presumably derived from nonenzymatic conversion of IAA) observed in buffer only, empty vector, and inactivated (boiled) enzyme controls (Fig. 1*C*). The calculated enzymatic activity of rDAO1 was 6.5 ± 0.2 pmol $oxIAA^{-1}$ min^{-1} mg protein, and rDAO2 was 6.3 ± 1.1 pmol $oxIAA^{-1}$ min^{-1} mg protein. These rates are consistent with the IAA oxidation rate previously observed in planta, which is between 10 and 40 nM^{-1} h (28), and indirectly support the hypothesis that DAO1 and DAO2 function in IAA oxidation in planta.

DAO1 Mutants Show Altered Auxin Metabolites and Auxin-Related Phenotypes

DAO1 and *DAO2* IAA oxidation activity was investigated in planta using reverse genetics. *DAO1* and *DAO2* are located in tandem on chromosome 1, with 1,091 bp between the stop codon of *DAO1* and the start codon of *DAO2*. Transfer-DNA (T-DNA) insertional mutants for *DAO1* and *DAO2* were obtained (29) and verified (Fig. 2 *A* and *B*). Quantitative real-time PCR (qPCR) showed that *DAO1* transcripts were not detected in *dao1-1* (first exon insertion), were reduced to 10% of the wild type in *dao1-3* (promoter insertion), and increased 1.7-fold in *dao1-2D* (3′ UTR insertion) compared with the wild type (Fig. 2 *A* and *B*). qPCR showed that *DAO2* expression was 61% less in *dao2-1* than the wild type (Fig. 2*B*). Seven-day-old mutant seedlings were analyzed for altered auxin metabolism, and *dao1-1* and *dao1-3* mutants exhibited 94.3% and 41.6% decreases in oxIAA production, respectively, whereas *dao1-2D* gain of function seedlings showed an 83% increase in oxIAA levels compared with the wild type [Columbia-0 (Col-0); $P < 0.001$] (Fig. 2*C*). Furthermore, the oxIAA levels in *dao1-1* were restored to wild type by the expression of native promoter-driven YFP-DAO1 ($dao1\text{-}1_{c6}$ and $dao1\text{-}1_{c11}$) (Fig. S5), although transcript abundance was greater than wild type. However, oxIAA accumulation in whole seedlings of the *dao2-1* knockdown line was not different from wild type ($P > 0.05$) (Fig. S6). Together, these data indicate that DAO1 is the primary IAA oxidase during seedling establishment.

Although the amount of free IAA was not significantly altered in *dao1-1* or *dao1-3* ($P > 0.05$) (Fig. 2*C*), two of the major IAA-amino acid conjugates, IAA-Asp and IAA-Glu, were substantially increased in *dao1-1* and *dao1-3* compared with wild type (Fig. 2*C*), consistent with the levels reported in the work by Porco et al. (24). The accumulation of IAA-Asp and IAA-Glu was noteworthy, because levels of these metabolites were below the limit of detection in wild type. Furthermore, Gretchen Hagen3.3 (*GH3.3*), which can synthesize IAA-Asp, was up-regulated in *dao1* loss of function mutants (Fig. S7) as noted by Porco et al. (24) and predicted by Mellor et al. (25). These data suggest that the IAA-amino acid conjugation pathway is induced to compensate for loss of DAO-mediated attenuation of auxin signaling.

However, the increased irreversible IAA conjugation was apparently not sufficient to complement the loss of IAA oxidase activity, because both *dao1-1* and *dao1-3* showed altered morphological phenotypes (Figs. 3 and 4) similar to those reported in the work by Porco et al. (24). Those morphological phenotypes were reminiscent of those observed in *yuc6-1D* (*kidari*), in which auxin levels are slightly elevated, and the expression domain of the *YUCCA6* auxin biosynthetic gene, normally restricted to flowers, carpels, pollen, and the root tip (30, 31), is expanded

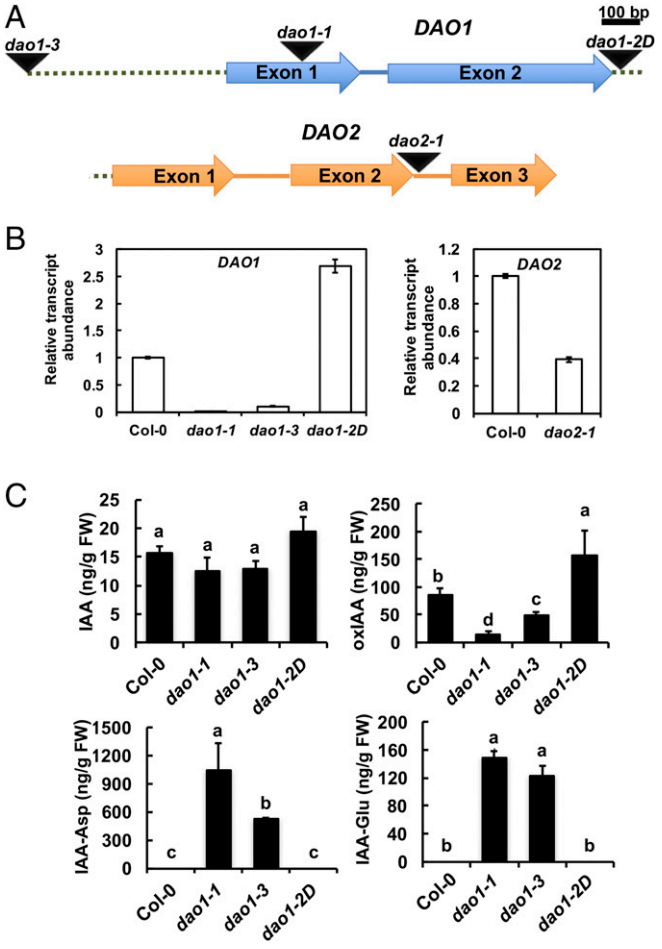

Fig. 2. Identification of *DAO1* and *DAO2* T-DNA insertion lines. (*A*) Gene organization and schematic representation of T-DNA insertion lines of *DAO1* (At1G14130) and *DAO2* (At1G14120). Arrows, exons; dotted line, 1,091-bp interval between *DAO1* stop codon and *DAO2* start codon; intervening lines, introns; triangles, T-DNA sites. (*B*) Transcript abundance of *DAO1* and *DAO2* in mutants compared with Col-0. (*C*) IAA and IAA metabolite concentrations in 7-d-old Col-0 (wild type) and mutant seedlings. Data are means ± SD of at least four biological repeats. Different letters indicate statistical significance (ANOVA; $P < 0.05$). FW, fresh weight.

into other vegetative organs (32, 33). When *dao1-1*, *dao1-3*, and *yuc6-1D* were compared with wild type, significant ($P < 0.001$) increases in lateral root density (+86%, 47%, and 85%, respectively) were observed (Fig. 3 *A* and *B*). Primary roots in young *dao1-1* and *dao1-3* seedlings were initially longer than the wild type, with root hair phenotypes similar to those reported by Porco et al. (24), but primary roots were not different in length compared with wild type at 11 d (Fig. S8). Root hairs in *yuc6-1D* were also elongated, but primary roots were 13% shorter than the wild type ($P < 0.05$).

Both *dao1-1* and *dao1-3* had planar and significantly larger cotyledons than the wild type (38% and 35%, respectively; $P < 0.05$) (Fig. 3 *C* and *D*). In 3-d-old etiolated seedlings, the hypocotyls of *dao1-1*, *dao1-3*, and *yuc6-1D* seedlings were 22%, 14%, and 19% longer than wild type, respectively ($P < 0.01$) (Fig. 3 *E* and *F*), with 14.5%, 15.5%, and 40% reductions in the apical hook angle in 3-d-old etiolated seedlings, respectively ($P < 0.001$) (Fig. 3*G*). Tropic responses were also altered in *dao1-1*, and root gravitropic bending and phototropic bending in postphotomorphogenic seedlings were faster in *dao1-1* than wild type during the initial stages of the tropic response ($P < 0.01$ and $P < 0.03$, respectively) (Fig. S9 and Movies S1 and S2).

Rosette radii in *dao1-1* and *dao1-3* were larger than the wild type (15.5% and 17%, respectively; $P < 0.01$) (Fig. 3 *H* and *I*) and contrasted strongly with the narrow and curling rosette leaves in *yuc6-1D*. Primary inflorescences were 35% longer in *dao1-1* and 27% longer in *dao1-3* than the wild type at 32 d ($P < 0.001$) (Fig. 3 *J* and *K*), similar to those in *yuc6-1D*. In contrast, the dominant mutant *dao1-2D* had smaller and rounder rosette leaves and shorter inflorescences compared with the wild type ($P < 0.001$) (Fig. S10). All of the loss of function phenotypes were restored to wild type in *dao1-1*$_{c6}$ and *dao1-1*$_{c11}$ YFP-DAO1 expression lines (Fig. 3). The knockdown mutant *dao2-1* had no obvious phenotypes (Fig. S11). Differences in the phenotypes reported here and in the work by Porco et al. (24) can be attributed to light intensity. Here, plants were grown under light conditions that result in lower

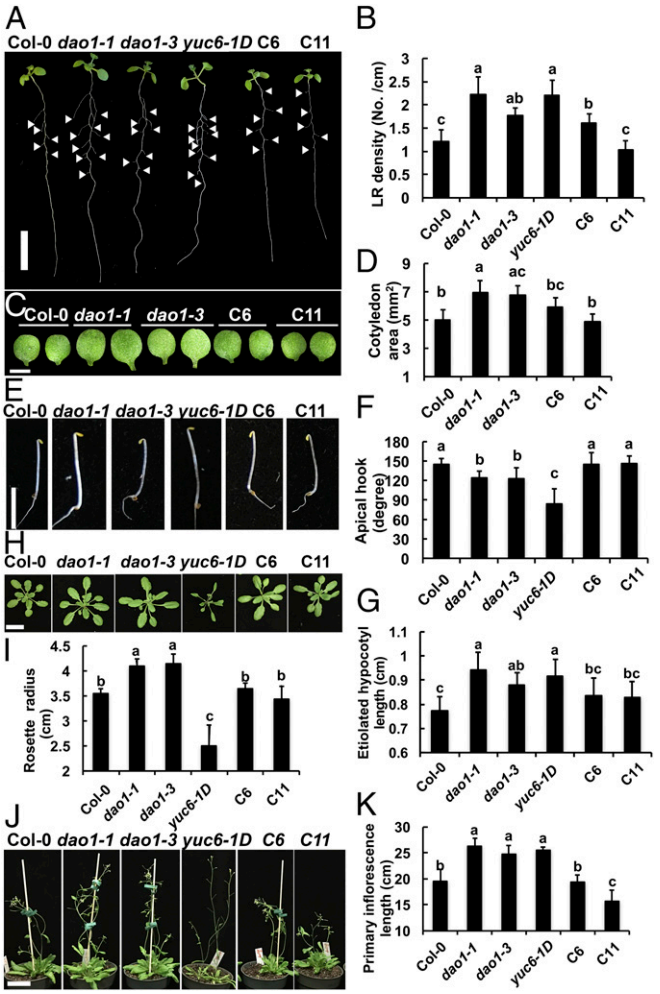

Fig. 3. *DAO1* loss of function plants show altered phenotypes and *dao1* complementation. Phenotypes of Col-0, *dao1-1*, *dao1-3*, *yuc6-1D*, and *dao1-1* complemented lines (C6 and C11). (*A*) Nine-day-old light-grown seedlings. (*B*) Quantification of lateral root (LR) density in 9-d-old seedlings. (*C* and *D*) Cotyledons from 7-d-old seedlings and quantification of cotyledon area. (*E*) Three-day-old etiolated seedlings. (*F* and *G*) Quantification of hypocotyl length and apical hook angle of 3-d-old etiolated seedlings. (*H*) Rosette leaves at bolting. (*I*) Rosette radii at bolting. (*J*) Thirty-two–day-old plants. (*K*) Primary inflorescence length of 32-d-old plants. Data are means ± SD ($n \geq 10$). Different letters indicate statistical significance (ANOVA; $P < 0.05$). (Scale bars: *A* and *H*, 1 cm; *C*, 0.5 cm; *J*, 5 cm.)

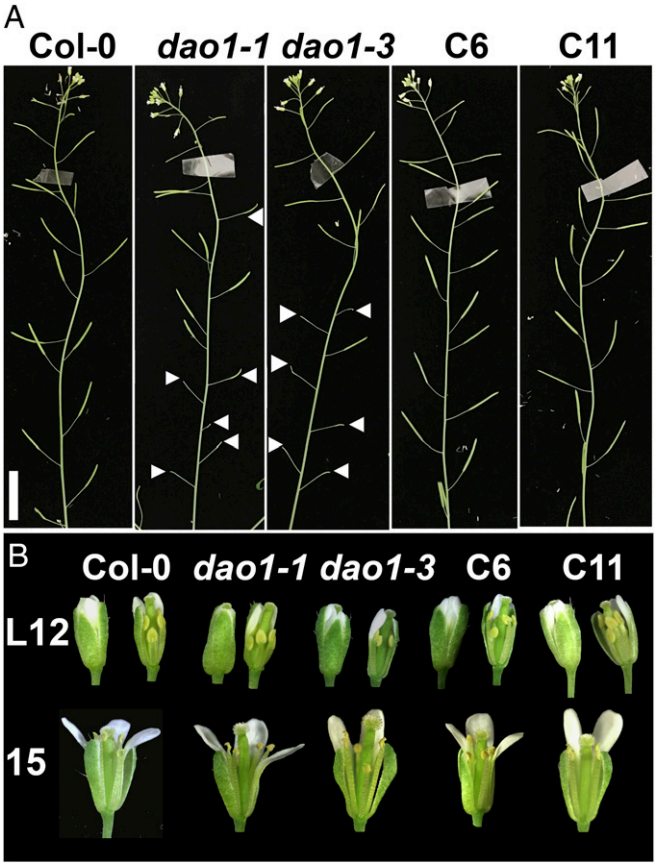

Fig. 4. Comparison of fertility and floral phenotypes of *dao1* mutants and complementation lines. (*A*) Primary inflorescences from 36-d-old Col-0, *dao1-1*, and complemented lines (C6 and C11). (*B*) Floral anatomy at late stage 12 (L12) and stage 15; L12 (*Left*) shows intact flowers, and in L12 (*Right*) and 15, sepals and petals were removed to show the pistil.

basal IAA levels (100 μmol m^{-2} s^{-1}), which seems to accentuate some of the observed phenotypes.

As also reported by Porco et al. (24), *dao1* loss of function mutants had small siliques with incomplete filling in an irregular pattern in the primary inflorescence (Fig. 4*A*). Closer investigation revealed that sepal opening was delayed at floral stage 13 in *dao1-1* mutants (Fig. 4*B*). Furthermore, at floral stage 15, the pistils in *dao1-1* and *dao1-3* were elongated compared with the wild type, resulting in variable pollination. These phenotypes are strong in primary inflorescences at the beginning of bolting but weaken later, especially in axillary inflorescences. These results are consistent with the concentration dependence of auxin metabolism levels during floral development and tissue specificity of DAO1 function. Together, these results support the hypothesis that DAO1 functions as an IAA oxidase in vivo and regulates plant morphogenesis.

DAO1 Is Expressed Throughout the Plant, and DAO2 Is Expressed in the Root Cap

The spatial and temporal expression patterns of DAO1 and DAO2 were examined to determine when and where DAO activity was required to maintain auxin homeostasis during growth and development. Microarray and transcriptomic analyses showed that *Arabidopsis DAO1* is expressed in reproductive organs (33, 34). *DAO1* is also expressed in the cortical, endodermal, and pericycle cells of the root distal elongation zone and maturation zone, the root columella, and atrichoblasts (35, 36). *DAO2* is expressed weakly in the root columella and procambium of the root maturation zone (35, 36). Transcriptomic data also indicate that *DAO2* expression in the root is several hundred fold lower than *DAO1* expression in the roots of *Arabidopsis* seedlings (36). These expression data are consistent with results of the accumulation profiles of IAA metabolites in *dao1-1* and *dao2-1* in seedlings (Fig. 2*C* and Fig. S6) (24, 25) but also suggest that some posttranslational regulation of DAO is likely.

DAO1 and DAO2 spatiotemporal expression patterns were analyzed using *DAO* native promoter-driven reporter and functional *DAO* fluorescent protein fusion constructs [*DAO1*pro:β-glucuronidase (GUS), *DAO1*pro:YFP-DAO1, and *DAO2*pro:YFP-DAO2]. Strong and constitutive *DAO1*pro:GUS activity was observed at the cotyledon margins and ubiquitously in the epidermis and vascular tissue in 7-d-old seedlings (Fig. 5*A*). These results are consistent with the larger cotyledons and leaves observed in *dao1-1* and *dao1-3* (Fig. 3 *C* and *D*) and the smaller leaves in *dao1-2D*, indicating that localized auxin oxidation mediated by DAO1 is involved in controlling cotyledon and leaf size. GUS activity had a distinct delineation at the root–shoot transition zone, where the adjacent root cells had little or no activity, whereas the adjacent shoot epidermal cells showed strong staining. These patterns are consistent with the florescence signals of *DAO1*pro:YFP-DAO1 in *dao1-1* seedlings. Confocal

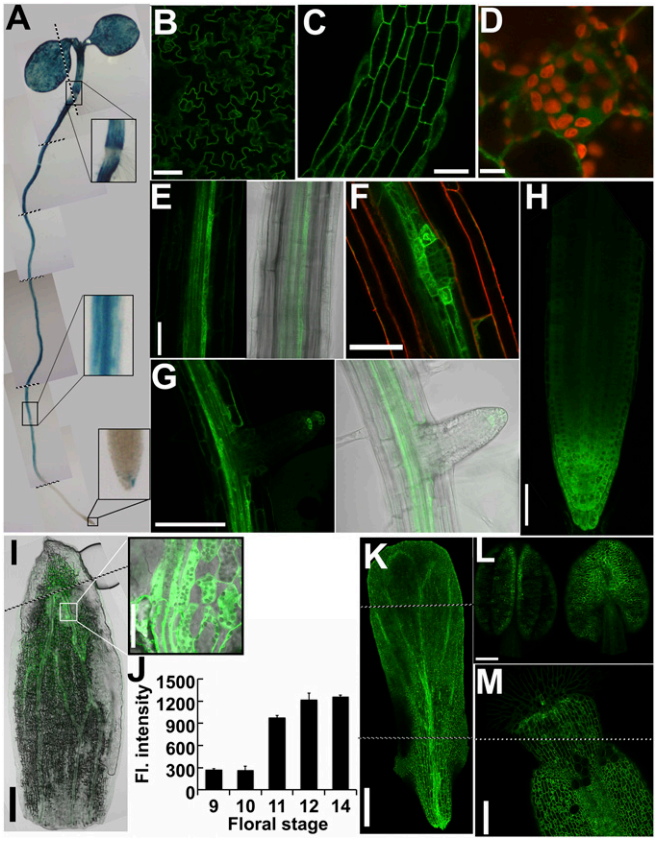

Fig. 5. Spatial and temporal expression pattern of *DAO1*. (*A*) *DAO1pro*:GUS activity in 7-d-old seedling. The boxes show magnified regions as indicated. (*B–E* and *G*) *DAO1pro*:YFP-DAO1 signals in 5-d-old seedling. (*B*) Cotyledon, (*C*) hypocotyl, and (*D*) subcellular localization of DAO1 in hypocotyl epidermis. Red indicates chloroplast autofluorescence. (*E*) Upper root. (*F*) Upper root with a lateral root primordium in a 9-d-old seedling. Red indicates FM4-64, a plasma membrane dye. (*G*) Lateral root in the 9-d-old seedling. (*H*) Primary root tip. (*I–M*) *DAO1pro*:YFP-DAO1 signals in floral stage 12. (*I*) Sepal. (*J*) Florescence intensity of *DAO1pro*:YFP-DAO1 in the upper sepal during flower development. Data are means ± SD. (*K*) Petal, (*L*) stamen, and (*M*) stigma. [Scale bars: *B*, *C*, *E–H*, and *I* (*Inset*), 0.5 mm; *D*, 0.01 mm; *I* and *L*, 0.2 mm; *K* and *M*, 0.1 mm.]

microscopy (Fig. 5 *B*–*G* and autofluorescence controls in Fig. S12) of 7-d-old seedlings showed cytosolic *DAO1*pro:YFP-DAO1 signals in the pavement cells of cotyledons, the epidermis, and the pericycle in the root and in the root cap. Porco et al. (24) also showed soluble DAO1-GFP signals in the root tip, pericycle, and trichoblasts. The YFP-DAO1 signal was much stronger in the pericycle cells flanking the developing lateral root primordia, and this pattern was maintained throughout the stages of lateral root development. However, no DAO1 signals were detectable in the tips of lateral roots until they emerged from the primary root (Fig. 5 *F* and *G*). The localization of DAO1 at the organ borders was similar to that observed at the root–shoot junction (Fig. 5*A*) and suggests a role in organ delineation.

Coinciding with DAO1 signals in the root cap, the DR5:GUS indirect auxin reporter construct in the *dao1-1* mutant showed enhanced activity in the root cap compared with the wild type (Fig. S13), a phenotype predicted by the modeling of auxin distribution in *dao1* loss of function mutants (25). These data support the hypothesis that localized IAA oxidation plays an important role in the regulation of auxin signaling in the root cap. Furthermore, in etiolated seedlings, YFP-DAO1 signals were greater on the inside of the apical hook, where DR5:GFP signals were also strong (Fig. S14), suggesting that DAO1 functions in apical hook maintenance. In contrast, analyses of YFP-DAO2 patterns showed that DAO2 signals were only weakly detected in the root cap of seedlings (Fig. S15 with autofluorescence controls), consistent with the low transcript levels of *DAO2* detected in the root and other tissues (36) (arexdb.org).

In floral organs, YFP-DAO1 signals were strongest in the sepal and petal vasculature as well as in the epidermis of all four whorls (Fig. 5 *I*–*M*). *DAO1* was strongly expressed near the sepal apex, especially in the bundle sheath cells and adjacent mesophyll cells just before flower opening (Fig. 3 *J* and *K* and autofluorescence controls in Fig. S12). This result is consistent with microarray data showing that *DAO1* expression in the sepals is highest at floral stage 15 (34). Before bud opening, the sepal apex is curved inward around the other floral organs to maintain a closed flower that protects the developing reproductive organs (37). Auxin regulation of sepal opening was suggested by high expression of the rate-limiting auxin biosynthetic gene *YUCCA4* at the sepal apex of young flowers (30). The delayed flower opening observed in *dao1-1* (Fig. 4*A*) supports the notion that IAA oxidation in sepal bundle sheath cells plays an important role in controlling the timing of sepal opening. LC-MS determinations showed that auxin levels are high in the sepals of very young flowers (42 ± 3.4 pg mg^{-1}) and reduced (6.7 ± 2.9 pg mg^{-1}) by the time of bud opening, indicating that *YUCCA4* and *DAO1* expressions are coordinated to fine tune auxin levels during sepal opening. This finding is also consistent with a defect in lemma and palea opening associated with *DAO* loss of function in rice (21). Strong DAO1 signals in the carpel (Fig. 5 *L* and *M*) correlated with the elongated carpel observed and reduced fertility in *dao1-1* and *dao1-3* (Fig. 4 *A* and *B*). However, no severe defects in fertility were observed in *dao1-1*.

Discussion

In contrast to observations in rice, where *dao* mutants were shown to have defects limited to anther dehiscence, pollen growth, and seed development (21), the data presented here suggest that temporal- and tissue-specific degradation of auxin by DAO1 plays an important role in plant growth and development, including regulation of lateral root density, inflorescence height, and leaf and floral organ size, with subsequent effects on fertility (Figs. 3 and 4). Strong and uniform DAO1 localization in cotyledons correlates with the increased cotyledon size in *dao1* loss of function alleles, indicating that localized oxidation of auxin is involved in regulating cotyledon size. The strong localization of DAO1 in the pericycle (Fig. 5*E*) and the border cells flanking the lateral root primordia but not in lateral root primordia (Fig. 5*F*) indicate that DAO1 functions in the process that generates the localized auxin maxima involved in initiating lateral root formation.

Recently, IAA derived from the root cap was found to be involved in the prepatterning of lateral root formation (38). Xuan et al. (38) reported that IAA oscillation amplitudes in the root cap determined the prebranch sites of the lateral root. However, the role of auxin oxidation was not addressed in that study. Both *DAO1* and *DAO2* are expressed in root cap, and *dao1* mutants show increased lateral root density (Figs. 3*A* and 5 *A* and *G* and Fig. S11), supporting the hypothesis that auxin oxidation in the root cap plays an important role in lateral root initiation. Our data indicate that localized auxin oxidation by both DAO1 and DAO2 in the root cap is involved in the regulation of lateral root density, consistent with the results presented by Xuan et al. (38). The oscillations that induce lateral root development (38) also seem to have a modulating effect on circadian rhythms, and both oxIAA production and *DAO* expression levels have been shown to follow circadian patterns (22, 25). However, *DAO2* null and *dao1 dao2* double mutants are still needed to fully characterize the role of auxin oxidation in lateral root development. Unfortunately, the tight linkage of *DAO1* and *DAO2* prevents ready analysis of *dao1 dao2* double mutants, and so far, we have not been able to stably inactivate both *DAO1* and *DAO2* with CRISPR-Cas9 or amiRNA (artificial microRNA).

Arabidopsis is self-fertile, and before anthesis, the stamens extend above the stigma at floral stage 14 (39). This process requires highly coordinated filament and pistil elongation, which is achieved by differentially regulated auxin levels in the respective organs (30, 40). The *abcb1 abcb19* double auxin transporter mutant shows reduced fertility as a consequence of impaired filament elongation (41). Similarly, our results show that loss of IAA oxidation results in an extended growth phase of the pistil (40) (Fig. 4). This finding suggests that auxin homeostasis is synergistically regulated in stamens and pistils for subsequent pollination. Our study indicates that spatiotemporal auxin oxidation by DAO1 plays an important role in coordination of filament and pistil elongation by reducing active auxin levels in the carpel and thus, restraining pistil elongation.

Data presented here and in the work by Porco et al. (24) show that *GH3* gene expression increases as a result of loss of *DAO* function. Porco et al. (24) also show a decrease in the auxin precursor indole pyruvate in *dao1*, which suggests either a down-regulation of auxin biosynthetic genes expression or posttranslational regulation of the enzymes. The low substrate specificities (K_{cats}) of auxin biosynthetic enzymes (30) and membrane localization of YUCCA isoforms suggest the possibility of functional, membrane-associated metabalons (42, 43). The slow kinetics of the DAOs are more similar to those of the auxin biosynthetic enzymes than to the those observed with GH3s. Accordingly, we hypothesize that DAO functions in tandem with the auxin biosynthetic machinery and may be recruited to the metabolon to fine tune auxin levels. Our data indicate that precise cooperation between IAA biosynthesis and IAA oxidation allows dynamic regulation of IAA levels that is likely required for flower development and lateral root formation.

These results presented here and in the works by Porco et al. (24) and Mellor et al. (25) also show that the irreversible major IAA conjugates, IAA-Glu and IAA-Asp, occur at higher levels in *dao1* loss of function alleles than in wild type (Fig. 2*C*). So why did plants evolve two different pathways to catabolize auxin and terminate auxin signaling? A functional comparison suggests that Asp conjugation is a rapid response, whereas auxin oxidation via DAO represents a constitutive mechanism to slowly remove auxin signals. The *GH3* family genes that encode the amino acid transferases are expressed at very low levels under normal growth conditions but are stimulated by application of exogenous auxin [*GH3.1, 2, 3, 4, 6*; Gene Expression Omnibus (GEO) accession no. GSM9969], blue light (*GH3.10*) (44), or jasmonic acid treatment (*GH3.9*) (45). *GH3* genes are among the fastest to respond to exogenous auxin, with

transcript levels increasing more than 10 times within 1 h (GEO accession no. GSM9969). Most *GH3* KO mutants (6) are hypersensitive to long-term exogenous IAA treatment. In contrast, *DAO1* has a constitutively high expression level in most tissues under normal conditions. In addition, GH3s have faster enzyme kinetics compared with DAOs from in vitro enzyme assays (6) (Fig. 1). Recombinant GH3.6 conjugates Asp to IAA at 244 nmol IAA-Asp min^{-1} mg^{-1} protein (6), whereas rDAO1 oxidizes IAA at 5 pmol $oxIAA^{-1}$ min^{-1} mg protein (Fig. 1*C*), more than 10,000 times slower than GH3.6 (6). Therefore, DAO1 seems to function spatiotemporally to terminate active auxin constitutively during development in contrast to GH3, which responds quickly to environmental factors that increase cellular IAA levels. This finding also explains why increased irreversible auxin conjugates in *dao1-1* could not compensate for the altered morphological phenotypes (24). Taken together, our results show that DAO1 regulates IAA homeostasis in a manner different from IAA conjugation and is functionally important in plant growth and development.

More details are in *SI Materials and Methods*.

ACKNOWLEDGMENTS. We thank Candace Pritchard for assistance with the phototropism assays; Sarah Turner and Jongmi Park for assistance with enzyme assays, RNA extractions, and growing plants; Dr. Angus Murphy for providing the auxin quantitation data in the sepals, helpful discussions, and critically reading the manuscript; and Dr. Jeong-Im Kim for the *yuc6-1D* seeds and discussion of the phenotypes. This work was supported by the Maryland Agricultural Research Station, the University of Maryland College of Agriculture and Natural Resources, and the Ohio Agricultural Research and Development Center SEEDS Grant Program, The Ohio State University, and Coordenação de Aperfeiçoamento de Pessoa de Nível Superior (Capes), Brazil.

1. Mashiguchi K, et al. (2011) The main auxin biosynthesis pathway in *Arabidopsis*. *Proc Natl Acad Sci USA* 108(45):18512–18517.
2. Stepanova AN, et al. (2011) The *Arabidopsis* YUCCA1 flavin monooxygenase functions in the indole-3-pyruvic acid branch of auxin biosynthesis. *Plant Cell* 23(11):3961–3973.
3. Jackson RG, et al. (2001) Identification and biochemical characterization of an *Arabidopsis* indole-3-acetic acid glucosyltransferase. *J Biol Chem* 276(6):4350–4356.
4. Jackson RG, et al. (2002) Over-expression of an *Arabidopsis* gene encoding a glucosyltransferase of indole-3-acetic acid: Phenotypic characterisation of transgenic lines. *Plant J* 32(4):573–583.
5. Tognetti VB, et al. (2010) Perturbation of indole-3-butyric acid homeostasis by the UDP-glucosyltransferase UGT74E2 modulates *Arabidopsis* architecture and water stress tolerance. *Plant Cell* 22(8):2660–2679.
6. Staswick PE, et al. (2005) Characterization of an *Arabidopsis* enzyme family that conjugates amino acids to indole-3-acetic acid. *Plant Cell* 17(2):616–627.
7. Ludwig-Müller J (2011) Auxin conjugates: Their role for plant development and in the evolution of land plants. *J Exp Bot* 62(6):1757–1773.
8. Korasick DA, Enders TA, Strader LC (2013) Auxin biosynthesis and storage forms. *J Exp Bot* 64(9):2541–2555.
9. Ishimaru K, et al. (2013) Loss of function of the IAA-glucose hydrolase gene TGW6 enhances rice grain weight and increases yield. *Nat Genet* 45(6):707–711.
10. Östin A, Kowalyczk M, Bhalerao RP, Sandberg G (1998) Metabolism of indole-3-acetic acid in *Arabidopsis*. *Plant Physiol* 118(1):285–296.
11. LeClere S, Tellez R, Rampey RA, Matsuda SPT, Bartel B (2002) Characterization of a family of IAA-amino acid conjugate hydrolases from *Arabidopsis*. *J Biol Chem* 277(23):20446–20452.
12. Rampey RA, et al. (2004) A family of auxin-conjugate hydrolases that contributes to free indole-3-acetic acid levels during *Arabidopsis* germination. *Plant Physiol* 135(2):978–988.
13. Ray PM (1958) Destruction of auxin. *Annu Rev Plant Physiol* 9(1):81–118.
14. Kowalczyk M, Sandberg G (2001) Quantitative analysis of indole-3-acetic acid metabolites in *Arabidopsis*. *Plant Physiol* 127(4):1845–1853.
15. Pencík A, et al. (2013) Regulation of auxin homeostasis and gradients in *Arabidopsis* roots through the formation of the indole-3-acetic acid catabolite 2-oxindole-3-acetic acid. *Plant Cell* 25(10):3858–3870.
16. Sandberg G, Ernstsen A (1987) Dynamics of indole-3-acetic acid during germination of *Picea abies* seeds. *Tree Physiol* 3(2):185–192.
17. Reinecke DM, Bandurski RS (1988) Oxidation of indole-3-acetic acid to oxindole-3-acetic acid by an enzyme preparation from *Zea mays*. *Plant Physiol* 86:868–872.
18. Hu T, Dryhurst G (1997) Electrochemical and peroxidase O2-mediated oxidation of indole-3-acetic acid at physiological pH. *J Electroanal Chem* 432(1-2):7–18.
19. Normanly J (1997) Auxin metabolism. *Physiol Plant* 100(3):431–442.
20. Peer WA, Cheng Y, Murphy AS (2013) Evidence of oxidative attenuation of auxin signalling. *J Exp Bot* 64(9):2629–2639.
21. Zhao Z, et al. (2013) A role for a dioxygenase in auxin metabolism and reproductive development in rice. *Dev Cell* 27(1):113–122.
22. Voß U, et al. (2015) The circadian clock rephases during lateral root organ initiation in *Arabidopsis thaliana*. *Nat Commun* 6:7641.
23. Butler ED, Gallagher TF (2000) Characterization of auxin-induced ARRO-1 expression in the primary root of *Malus domestica*. *J Exp Bot* 51(351):1765–1766.
24. Porco S, et al. (2016) Dioxygenase-encoding *AtDAO1* gene controls IAA oxidation and homeostasis in *Arabidopsis*. *Proc Natl Acad Sci USA* 113:11016–11021.
25. Mellor N, et al. (2016) Dynamic regulation of auxin oxidase and conjugating enzymes *AtDAO1* and *GH3* modulates auxin homeostasis. *Proc Natl Acad Sci USA* 113: 11022–11027.
26. Dinkel H, et al. (2016) ELM 2016–data update and new functionality of the eukaryotic linear motif resource. *Nucleic Acids Res* 44(D1):D294–D300.
27. Durek P, et al. (2010) PhosPhAt: *The Arabidopsis thaliana* phosphorylation site database. An update. *Nucleic Acids Res* 38(Database issue):D828–D834.
28. Kramer EM, Ackelsberg EM (2015) Auxin metabolism rates and implications for plant development. *Front Plant Sci* 6(March):150.
29. Alonso JM, et al. (2003) Genome-wide insertional mutagenesis of *Arabidopsis thaliana*. *Science* 301(5633):653–657.
30. Cheng Y, Dai X, Zhao Y (2006) Auxin biosynthesis by the YUCCA flavin monooxygenases controls the formation of floral organs and vascular tissues in *Arabidopsis*. *Genes Dev* 20(13):1790–1799.
31. Kim JI, et al. (2007) yucca6, a dominant mutation in *Arabidopsis*, affects auxin accumulation and auxin-related phenotypes. *Plant Physiol* 145(3):722–735.
32. Kim JI, et al. (2011) YUCCA6 over-expression demonstrates auxin function in delaying leaf senescence in *Arabidopsis thaliana*. *J Exp Bot* 62(11):3981–3992.
33. Swanson R, Clark T, Preuss D (2005) Expression profiling of *Arabidopsis* stigma tissue identifies stigma-specific genes. *Sex Plant Reprod* 18(4):163–171.
34. Schmid M, et al. (2005) A gene expression map of *Arabidopsis thaliana* development. *Nat Genet* 37(5):501–506.
35. Winter D, et al. (2007) An "Electronic Fluorescent Pictograph" browser for exploring and analyzing large-scale biological data sets. *PLoS One* 2(8):e718.
36. Brady SM, et al. (2007) A high-resolution root spatiotemporal map reveals dominant expression patterns. *Science* 318(5851):801–806.
37. Takeda S, et al. (2013) Physical interaction of floral organs controls petal morphogenesis in *Arabidopsis*. *Plant Physiol* 161(3):1242–1250.
38. Xuan W, et al. (2015) Root cap-derived auxin pre-patterns the longitudinal axis of the *Arabidopsis* root. *Curr Biol* 25(10):1381–1388.
39. Smyth DR, Bowman JL, Meyerowitz EM (1990) Early flower development in *Arabidopsis*. *Plant Cell* 2(8):755–767.
40. Tashiro S, Tian CE, Watahiki MK, Yamamoto KT (2009) Changes in growth kinetics of stamen filaments cause inefficient pollination in massugu2, an auxin insensitive, dominant mutant of *Arabidopsis thaliana*. *Physiol Plant* 137(2):175–187.
41. Titapiwatanakun B, et al. (2009) ABCB19/PGP19 stabilises PIN1 in membrane microdomains in *Arabidopsis*. *Plant J* 57(1):27–44.
42. Müller A, Weiler EW (2000) IAA-synthase, an enzyme complex from *Arabidopsis thaliana* catalyzing the formation of indole-3-acetic acid from (S)-tryptophan. *Biol Chem* 381(8):679–686.
43. Kriechbaumer V, Botchway SW, Hawes C (2016) Localization and interactions between *Arabidopsis* auxin biosynthetic enzymes in the TAA/YUC-dependent pathway. *J Exp Bot* 67(14):4195–4207.
44. Takase T, et al. (2004) ydk1-D, an auxin-responsive GH3 mutant that is involved in hypocotyl and root elongation. *Plant J* 37(4):471–483.
45. Khan S, Stone JM (2007) *Arabidopsis thaliana* GH3.9 in auxin and jasmonate cross talk. *Plant Signal Behav* 2(6):483–485.
46. Ulmasov T, Liu ZB, Hagen G, Guilfoyle TJ (1995) Composite structure of auxin response elements. *Plant Cell* 7(10):1611–1623.
47. Ottenschläger I, et al. (2003) Gravity-regulated differential auxin transport from columella to lateral root cap cells. *Proc Natl Acad Sci USA* 100(5):2987–2991.
48. Laemmli UK (1970) Cleavage of structural proteins during the assembly of the head of bacteriophage T4. *Nature* 227(5259):680–685.
49. Novák O, et al. (2012) Tissue-specific profiling of the *Arabidopsis thaliana* auxin metabolome. *Plant J* 72(3):523–536.
50. Grefen C, et al. (2010) A ubiquitin-10 promoter-based vector set for fluorescent protein tagging facilitates temporal stability and native protein distribution in transient and stable expression studies. *Plant J* 64(2):355–365.
51. Clough SJ, Bent AF (1998) Floral dip: A simplified method for *Agrobacterium*-mediated transformation of *Arabidopsis thaliana*. *Plant J* 16(6):735–743.
52. Schneider CA, Rasband WS, Eliceiri KW (2012) NIH Image to ImageJ: 25 years of image analysis. *Nat Methods* 9(7):671–675.
53. Geisler M, et al. (2005) Cellular efflux of auxin catalyzed by the *Arabidopsis* MDR/PGP transporter AtPGP1. *Plant J* 44(2):179–194.
54. Murphy A, Taiz L (1999) Localization and characterization of soluble and plasma membrane aminopeptidase activities in *Arabidopsis* seedlings. *Plant Physiol Biochem* 37(6):431–443.
55. Larkin MA, et al. (2007) Clustal W and Clustal X version 2.0. *Bioinformatics* 23(21):2947–2948.
56. Tamura K, Stecher G, Peterson D, Filipski A, Kumar S (2013) MEGA6: Molecular Evolutionary Genetics Analysis version 6.0. *Mol Biol Evol* 30(12):2725–2729.